



Asymmetry and pathways of inter-hemispheric transport in the upper troposphere and lower stratosphere

Xiaolu Yan^{1,a}, Paul Konopka², Marius Hauck⁴, Aurélien Podglajen⁵, and Felix Ploeger^{2,3}

¹State Key Laboratory of Severe Weather & CMA Key Laboratory of Atmospheric Chemistry, Chinese Academy of Meteorological Sciences, Beijing, China

²Institute for Energy and Climate Research: Stratosphere (IEK-7), Forschungszentrum Jülich, Jülich, Germany

³Institute for Atmospheric and Environmental Research, University of Wuppertal, Wuppertal, Germany

⁴Institute for Atmospheric and Environmental Sciences, Goethe University Frankfurt am Main, Frankfurt am Main, Germany

⁵Laboratoire de Météorologie Dynamique (LMD/IPSL), École polytechnique, Institut polytechnique de Paris, Sorbonne Université, École normale supérieure, PSL Research University, CNRS, Paris, France

^aformerly at: Institute for Energy and Climate Research: Stratosphere (IEK-7), Forschungszentrum Jülich, Jülich, Germany

Correspondence: Xiaolu Yan (xiaoluyan@cma.gov.cn)

Abstract. Inter-hemispheric transport may strongly affect the trace gas composition of the atmosphere, especially in relation to anthropogenic emissions which originate mainly in the Northern Hemisphere. This study investigates the transport from the boundary surface layer of the Northern Hemispheric (NH) extratropics (30-90° N), Southern Hemispheric (SH) extratropics (30-90° S), and tropics (30° S-30° N) into the global upper troposphere and lower stratosphere (UTLS) using simulations with the Chemical Lagrangian Model of the Stratosphere (CLaMS). In particular, we diagnose inter-hemispheric transport in terms of the air mass fractions (AMF), age spectra, and the mean age of air (AoA) calculated for these three source regions. We find that the AMFs from the NH extratropics to the UTLS are about five times larger than the corresponding contributions from the SH extratropics and almost twenty times smaller than those from the tropics. The amplitude of the AMF seasonal variability originating from the NH extratropics is comparable to that from the tropics. The NH and SH extratropics age spectra show much stronger seasonality compared to the seasonality of the tropical age spectra. The transit time of NH extratropical origin air to the SH extratropics is longer than vice versa. The asymmetry of the inter-hemispheric transport is mainly driven by the Asian summer monsoon (ASM). Both ASM and westerly ducts affect the cross hemispheric transport of the NH extratropical air to the SH, and it is an interplay between the ASM and westerly ducts which triggers such cross-equator transport from boreal summer to fall, mainly westerly ducts over the eastern Atlantic.

1 Introduction

The transport from the troposphere to the stratosphere plays an important role in determining the chemical composition of the atmosphere, and hence radiative features, which can impact atmospheric chemistry and global climate. For example, the ozone-depleting substances (ODS), greenhouse gases, and aerosols in the atmosphere are mainly driven by natural and anthropogenic emissions at the Earth's surface (e.g. Fueglistaler et al., 2004; WMO, 2018). Tropospheric air, which enters the stratosphere mainly through the tropical tropopause layer (TTL) (e.g. Holton et al., 1995; Levine et al., 2007; Fueglistaler et al., 2009),



is then transported to the global stratosphere by the Brewer-Dobson (BD) circulation (e.g. Butchart, 2014). Although most tropospheric air is transported to the stratosphere through the TTL driven by the BD circulation, significant contributions of air mass transport from troposphere to stratosphere through other pathways, e.g. monsoons (e.g. Randel et al., 2012; Ploeger et al., 2017), quasi-isentropic transport through the extratropics (e.g. Konopka et al., 2004; Hoor et al., 2005; Bönisch et al., 2009), and inter-hemispheric transport (e.g. Tomas and Webster, 1994; Waugh and Polvani, 2000; Orbe et al., 2018; Wu et al., 2018).

Inter-hemispheric transport is important for understanding the distributions of atmospheric tracers because of the asymmetry in anthropogenic emissions between the Southern Hemisphere (SH) and the Northern Hemisphere (NH), with generally strongest emissions in the NH caused by the higher population density. For instance, the anthropogenic and long-lived greenhouse gas SF₆ in the atmosphere, which is widely used in the study of transport (e.g. Maiss et al., 1996; Denning et al., 1999; Gloor et al., 2007; Patra et al., 2011; Krol et al., 2018), mostly originates from the NH (e.g. Ravishankara et al., 1993; Kovács et al., 2017). The ALE/GAGE experiment showed that nearly 95% of the reported sources of ODSs (e.g. CH₃CCl₃ and CFCl₃) are in the NH with maxima centred around the mid-latitudes (Wang and Shallcross, 2000). Besides the anthropogenic emissions, the natural emissions in the NH are different from those in the SH due to the asymmetry of topography and land-sea distribution between the two hemispheres. Although the source distributions of many tracers are different in the SH and NH, the observed trends of the tracers are almost homogeneous in the global upper troposphere and lower stratosphere (UTLS), which suggests the key role of inter-hemispheric transport in regulating the distribution of atmospheric trace gases and maintaining the mass balance (e.g. Müller and Brasseur, 1995; Wang and Shallcross, 2000; Liang et al., 2014; Patra et al., 2014; Chen et al., 2017). Francey and Frederiksen (2016) emphasised the importance of inter-hemispheric transport annual variations in explaining the sudden increase of the annual mean CO₂ difference between Mauna Loa in the NH and Cape Grim in the SH during 2009-2010.

A simplified model including two well mixed boxes respectively for the SH and the NH has been extensively used to quantify the inter-hemispheric transport in previous studies (e.g. Czeplak and Junge, 1975; Denning et al., 1999; Lintner et al., 2004; Patra et al., 2009; Chen et al., 2017; Krol et al., 2018; Naus et al., 2019). Due to the strong transport barrier between the tropics and extratropics (e.g. Hoskins et al., 1985; Bowman, 2006; Kunz et al., 2011; Ploeger et al., 2015; Poshyvailo et al., 2018), a three-box model including the SH extratropics, tropics, and NH extratropics was suggested to be used in quantifying inter-hemispheric transport (e.g. Bowman and Carrie, 2002; Erukhimova and Bowman, 2006). Many mechanisms have been proposed to drive the inter-hemispheric transport including transport related to eddies and wave breaking (e.g. Czeplak and Junge, 1975; Tomas and Webster, 1994; Staudt et al., 2001), vertical convective transport (e.g. Hartley and Black, 1995; Denning et al., 1999; Lintner et al., 2004; Erukhimova and Bowman, 2006), Hadley circulations (e.g. Bowman and Cohen, 1997; Wang and Shallcross, 2000), and monsoon circulations (e.g. Orbe et al., 2016; Chen et al., 2017). Zonally resolved results showed that westerly ducts over the Pacific and Atlantic regions are favored regions for the inter-hemispheric transport and redistribution of the atmospheric compositions (e.g. Webster and Holton, 1982; Tomas and Webster, 1994; Waugh and Polvani, 2000; Staudt et al., 2001; Ratnam et al., 2015; Francey and Frederiksen, 2016). The westerly ducts are strongest in boreal winter and affected by the El Niño Southern Oscillation (ENSO) events, which are stronger during La Niña periods and weaker during El Niño periods (e.g. Staudt et al., 2001; Dlugokencky et al., 2009; Francey and Frederiksen, 2016; Pandey et al., 2017).



The exchange time (τ_{ex}) across the equator is one common parameter to quantify the inter-hemispheric transport, and is defined by the mass balance equation derived from the difference of mean mixing ratios of tracers in the NH and SH and the net cross-equatorial flux (See e.g. Jacob et al., 1987; Patra et al., 2009; Waugh et al., 2013). τ_{ex} is related to the calculation method and to the hemispheric distribution and emissions of the tracer chosen. Values of τ_{ex} range between 0.8-2.0 yr based on the calculations of different models and passive tracers (e.g. Maiss et al., 1996; Denning et al., 1999; Peters et al., 2004; Patra et al., 2011; Liang et al., 2014; Yang et al., 2019). Age of air (AoA) is another widely used variable to quantify the inter-hemispheric transport, which provides more information compared to the inter-hemispheric exchange time τ_{ex} . AoA can be derived from the age spectrum, and has also been determined from observations of species with a nearly linear growth in mixing ratios such as for CO₂ and SF₆ (e.g. Hall and Plumb, 1994; Volk et al., 1997; Engel et al., 2009; Stiller et al., 2012; Ray et al., 2014; Engel et al., 2017) and from model simulations (e.g. Schoeberl et al., 2005; Garny et al., 2014; Konopka et al., 2015; Ploeger and Birner, 2016). These AoA calculations are sensitive to the tracers chosen, to the method of calculation and to the models and reanalysis data used (e.g. Krol et al., 2018; Fritsch et al., 2019; Hauck et al., 2019; Podglajen and Ploeger, 2019; Ploeger et al., 2019). Waugh et al. (2013) estimated AoA using SF₆ observations and showed that the mean AoA from the NH midlatitude surface to the SH midlatitudes is around 1.4 years. Orbe et al. (2016) and Chen et al. (2017) highlighted the important role of monsoon circulations in reducing mean AoA in the SH with respect to the NH. Konopka et al. (2017) and Krol et al. (2018) recently discussed an interesting asymmetry feature in inter-hemispheric transport with more effective transport from the NH surface to the SH than vice versa.

Most previous studies have examined the inter-hemispheric transport from the NH to the SH using a two-box model based on zonally mean results. However, the pathways and contributions of inter-hemispheric transport have not been well understood hitherto. Since anthropogenic emissions are mainly produced in the NH, the understanding of transport from the NH to the tropics, the SH, and the global stratosphere is particularly important. In this study, we address the following questions:

- (1) How large are the contributions from the SH, NH, and tropics to the upper troposphere and stratosphere, and what is the transit time?
- (2) Which regions are preferential/favored regions for the inter-hemispheric transport from the NH to the SH?
- (3) What is the underlying mechanism in terms of dynamics and circulation?

We investigate the transport from the NH to the SH and vice versa using the simulations from a three dimensional Chemical Lagrangian Model of the Stratosphere (CLaMS) with the atmospheric source regions divided into three domains (the SH extratropics, tropics, and NH extratropics). We quantify the contributions of air fractions and age spectra from these different regions. Particularly, we focus on quantifying the inter-hemispheric transport and characterising the pathways of inter-hemispheric transport by analysing zonally resolved model output. Section. 2 presents data and methods for our analyses. In Sect. 3, we diagnose the seasonality of transport from different source regions. We explore the pathways of inter-hemispheric transport in Sect. 4 and discuss our findings in Sect. 5 before closing with a summary of the key results in Sect. 6.



2 Data and methods

In this study, the surface is divided into 3 boxes to investigate the inter-hemispheric transport, which are the NH extratropics (30-90° N), SH extratropics (30-90° S), and tropics (30° S-30° N), respectively. We calculate age spectra and air mass fraction (AMF) to study transport from the surface of the NH extratropics, SH extratropics, and tropics using the CLaMS model. CLaMS is a Lagrangian chemistry transport model (CTM) with trace gas transport driven by horizontal winds and total diabatic heating rates from reanalysis data (e.g. McKenna et al., 2002; Konopka et al., 2004; Pommrich et al., 2014).

We apply the boundary impulse (time-) evolving response (BIER) approach to calculate the age spectrum G , following Ploeger and Birner (2016). Multiple tracer pulses are released in the boundary source region Ω_i , with i labeling the source domain (e.g., NH extratropics, SH extratropics, tropics). The passive tracer with mixing ratio χ at location r and time t related to the mixing ratio $\chi_0(t)$ from the boundary surface of different source regions, which defines the AMF from source regions, can be expressed as (e.g. Waugh and Hall, 2002; Ploeger et al., 2019):

$$\chi(r, t) = \int_0^\infty d\tau \chi_0(\Omega_i, t - \tau) G(r, t | \Omega_i, t - \tau) \quad (1)$$

The age spectrum is calculated from 120 inert pulse trace gas species from three source regions, with 40 different species pulsed from each region. These pulse tracers approximate a delta distribution lower boundary condition $\chi_0^j(\Omega_i, t) = \delta(t - t_j)$ with $j=1, \dots, 40$, defining tracer pulses at source times t_j . The pulse tracer mixing ratios are set to one in the boundary layer of the source region for 30 days, and are set to zero in the boundary layer outside of the initialization region in every time step. The first 24 different species ($j=1, \dots, 24$) with transit time less than 2 years are pulsed every month. The other 16 different species ($j=25, \dots, 40$) are pulsed every sixth month (e.g., 25th species in the 30th month, 26th species in the 36th month, etc.). Hence, all species have been pulsed after 10 years of model simulations, and are reset to zero in the whole atmosphere and pulsed again subsequently thereafter.

Therefore, the model simulations provide a monthly resolution age spectrum for transit times shorter than two years and a semi-annual resolution age spectrum for longer transit times. The integration of the spectrum over time generally yields a value less than 1 and AoA is young-biased caused by the truncation of the simulations at 10 years. Therefore, we calculate the mean AoA for each source region by normalizing the age spectrum to unit norm:

$$\Gamma(r, t) = \int_0^{10} \tau G(r, t | \Omega_i, \tau) d\tau / \int_0^{10} G(r, t | \Omega_i, \tau) d\tau \quad (2)$$

The details about the model setup and the calculation of age spectra from multiple pulse tracers and the mean AoA from the age spectrum can be found in Ploeger and Birner (2016) and Ploeger et al. (2019). For this study, we carried out a simulation covering the period from 1989 to 2017 with transport driven by the meteorological data from ERA-Interim (Dee et al., 2011). Due to the 10 year spin-up time for the age spectra, the model data from 1999-2017 is analyzed in the following to address the questions raised in the introduction.



3 Seasonality of transport

3.1 Seasonality of air mass fractions

120 To evaluate the contributions from the source regions, we calculate the zonally averaged seasonal mean of AMF from the boundary layer of the three source regions. In the following, we use the abbreviations of months (DJF, MAM, JJA, and SON) to represent different seasons. Figure 1 shows the seasonal variations in AMF originating from the NH extratropics (left), SH extratropics (middle), and tropics (right) during 1999-2017. The total sum of the AMF over all 3 source regions is ~ 1 related to the limitation of the maximal transit time in our simulations. For direct comparisons, we use the same colorbar for the AMF
125 transported from all the three source regions with different scaling factors. The global results show that the AMFs from the NH extratropics to the UTLS are about five times larger than the corresponding contributions from the SH extratropics and almost twenty times smaller than those from the tropics. Although the contributions from the tropics to the UTLS are much larger than those from the NH extratropics, the annual amplitude of tropical AMFs in the UTLS is comparable to that of NH extratropical AMFs related to the small contributions from the SH extratropics.

130 Newly pulsed air masses (younger than 3 months) from the NH extratropics start to cross the subtropical tropopause in boreal summer (JJA, Fig. 1g). Three months later, air masses from the NH extratropics are elevated to the lower stratosphere first mainly in the Asian summer monsoon (ASM) region driven by the monsoon circulation, and are then transported isentropically to the tropical lower stratosphere and NH extratropical lower stratosphere covering the latitude range from 30° S up to the Arctic regions (Fig. 1j). Later on, the NH extratropical air masses in the upper tropospheric and lower stratospheric tropics driven by
135 the ASM are further transported to the tropical pipe and the whole SH in DJF and MAM (Fig. 1a and Fig. 1d). Note that young air masses pulsed during boreal winter and spring (DJF and MAM) are not transported to the subtropical stratosphere.

The seasonality in the transport patterns of AMFs originating from the SH extratropics are shifted by 6 months compared to those from the NH extratropics. Although the respective contributions of the SH extratropics (i.e. in DJF and MAM) show some similarities to those from the NH extratropics (i.e. in JJA and SON), there are few significant differences between transport
140 from NH extratropics and SH extratropics. Crossing of the subtropical tropopause for SH extratropical origin air happens first in austral autumn (MAM, Fig. 1e) rather than austral summer (DJF, Fig. 1b), and the overall impact of the SH extratropical boundary surface tracers on both the tropics and the high latitudes is significantly weaker. Most transport of SH extratropical origin tracers is inhibited by the tropopause in the subtropical SH during DJF (Fig. 1b) and MAM (Fig. 1e). Especially, the SH extratropical AMF in the SH lower stratosphere during austral autumn (MAM) is much smaller than the NH extratropical
145 AMF in the NH lower stratosphere during boreal autumn (SON). These differences are most likely attributed to hemispheric differences in the strengths of the monsoons (e.g. Orbe et al., 2016; Chen et al., 2017) and in the strength and downward extent of the polar vortices.

Figure 1(right) shows that the tropical surface air dominates the atmospheric composition in the global UTLS. The seasonality of the tropical contribution results from the superposition of the Hadley and BD circulations, which are schematically
150 illustrated in Fig. 2 for DJF (a) and JJA (b) by using the residual mean mass stream function. The upwelling of the Hadley and BD circulations is shifted northward from DJF to JJA. Note the hemispheric asymmetric upwelling positions of the circula-

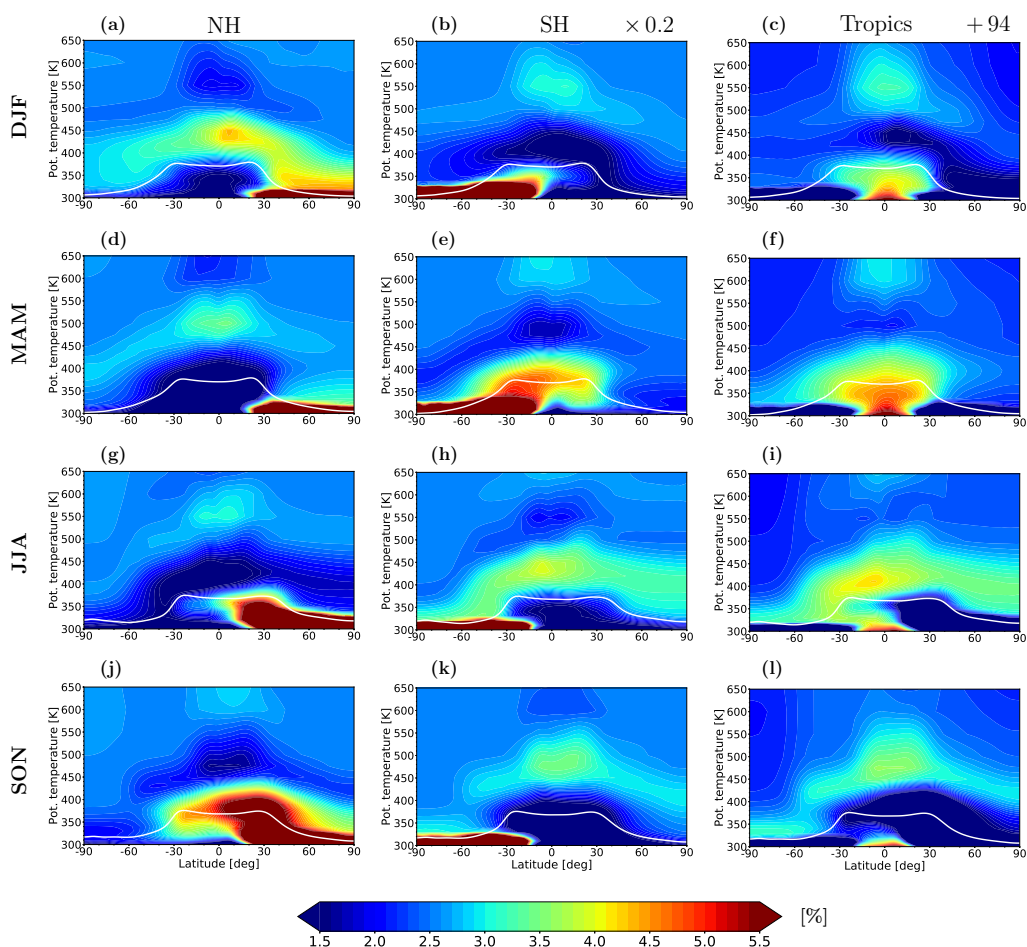


Figure 1. Climatological (1999-2017) zonal mean of the air mass fractions (AMFs) originated from the NH extratropics (30-90° N, left), SH extratropics (30-90° S, middle), and tropics (30° S-30° N, right) for DJF (top row), MAM (second row), JJA (third row), and SON (bottom row). The AMFs over all 3 source regions add up to ~1. The thick white line shows the (WMO) tropopause. Note that the colorbar is for the NH extratropical origin air, and the values in the colorbar should be multiplied by 0.2 for the SH extratropical origin air and plus 94 for the tropical origin air.

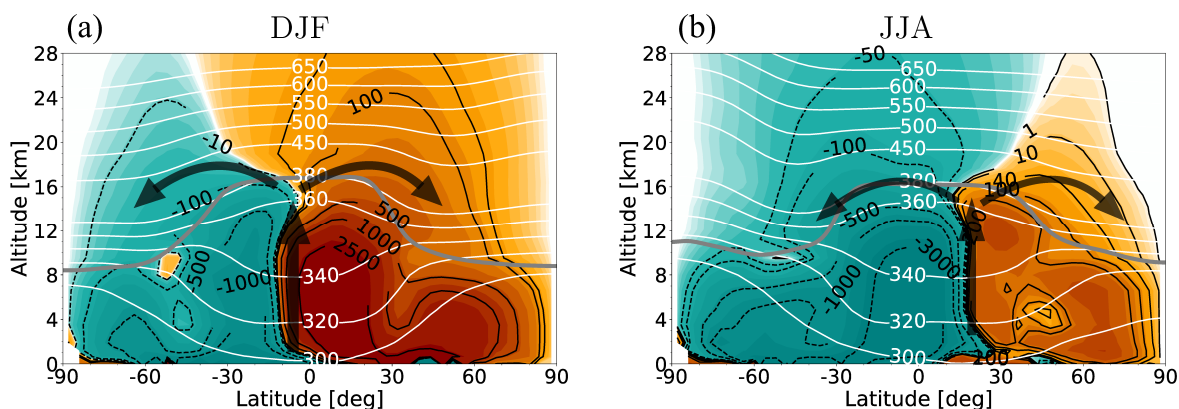


Figure 2. Climatology (1999-2017) of the residual mean mass streamfunction (colour shading) in DJF (a) and JJA (b) with positive and negative values marked with the black solid and dashed contours, respectively. The thick grey line shows the (WMO) tropopause, and thin white lines show potential temperature levels. The thick black arrows schematically illustrate the upwelling of the Hadley cell and the shallow branch of the BD circulation (around 400 K).

tions in winter and summer. The Hadley cell upwelling is located in the SH tropics around 5° S during boreal winter, while the upwelling is shifted far into the NH subtropics to latitudes of around 20° N in boreal summer. Thus, the strongest contribution of the tropical surface air to the stratosphere starts in boreal winter (DJF, Fig. 1c) and peaks in MAM (Fig. 1f) as the result of strongest positive coupling between the Hadley and BD circulation. The seasonality, in terms of relative amplitude, of the air originating from the tropics is less pronounced compared to that from the NH extratropics and SH extratropics. The evolution of the tropical source air shows similar patterns to those from the SH extratropics. The transport pattern is significantly different for transport from the NH extratropical source air. It is especially remarkable how the northward shift in the boreal summer Hadley cell weakens upward transport from the tropics during JJA and SON (Fig. 1i and Fig. 1j) while favouring upward transport from the NH surface (Fig. 2b), whereas this effect is much weaker during the austral summer (DJF and MAM, Fig. 1c and Fig. 1f).

To further explore the seasonal variations of transport from the boundary layer, we remove the annual mean of the contributions from each source region. These seasonal anomalies of climatological zonal mean AMF are shown in Fig. 3 respectively from the NH extratropics (left), SH extratropics (middle), and tropics (right). Clearly, the seasonality of air in the global UTLS originating from the NH extratropics is comparable to those from the tropics, and they are about five times larger than the corresponding anomalies from the SH extratropics being consistent with the results from Fig. 1.

Fig. 3 shows clear seasonal variations of AMF from each source region. The transport features of NH extratropical air anomalies starting from boreal summer (JJA) again show similar patterns to those from the SH extratropics starting from austral summer (DJF) with a shift of 6 months and much smaller anomalies. There are few new structures in Fig. 3 compared to the absolute contributions in Fig. 1. A pronounced positive anomaly in the lower stratosphere over the NH extratropics in SON (Fig. 3j) is related to the isentropic transport directly above the ASM region after the elevation of NH extratropical air

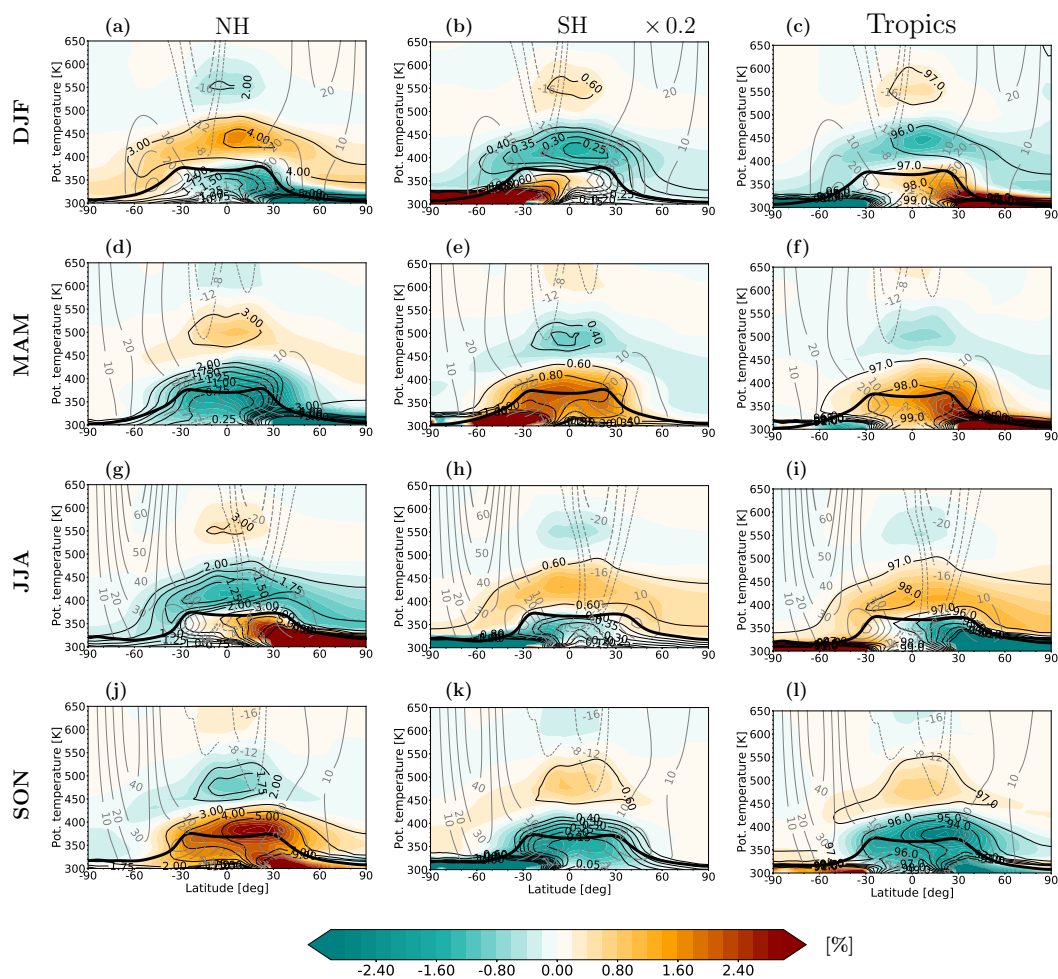


Figure 3. Climatological (1999-2017) zonal mean anomaly of AMF with the annual average removed (colour shading) originating from the NH extratropics (30-90° N, left), SH extratropics (30-90° S, middle), and tropics (30° S-30° N, right). The absolute contributions (black contours) from the source regions are also shown. The mean longitudinal winds are indicated by grey contours. The thick black line shows the (WMO) tropopause. Note the scale factor of colorbar for the SH extratropical origin air (0.2).



by the monsoon circulation, which again suggests that the tropospheric air in the NH extratropics is mainly transported to the NH and tropical lower stratosphere via the ASM circulation. Another striking feature is the negative anomaly of the NH extratropical air mass in the layer around 320 K in the NH during boreal autumn (Fig. 3j). This signature might be associated with the combination of less convective activity in boreal autumn in the NH extratropics, or with the suppression of horizontal transport from the subtropical troposphere in the layer around 320 K or, finally, with the southward movement of the Hadley cell enhancing isentropic, poleward transport from the tropics and across the still weak summer-autumn jet at levels above (see Fig. 3l).

In contrast to the NH case, the anomaly for SH extratropical air masses shows negative values almost throughout the SH extratropical lower stratosphere during austral autumn (Fig. 3e). This difference to the NH extratropical air (Fig. 3j) is mainly related to the weak convection and the strong inhibition (strong zonal jet) of horizontal transport from the subtropical region in the SH during austral autumn (MAM). In the NH, the tropopause barrier is weak and upward motion over the ASM region is strong, and a substantial amount of NH extratropical origin air can be transported to the lower stratosphere driven by monsoon circulations.

185 3.2 Seasonality of age spectrum and age of air

In Sec. 3.1, we have quantified transport using the AMF, which measures the contribution from different source regions to the air composition at a given destination point. In this section, we provide a complementary view of transport in terms of the age spectrum derived from the same simulations and for the same source regions as in Sec. 3.1. Figures 1 and 3 show that strong isentropic transport across the tropopause occurs in the layer around 360 K. Hence, we consider the age spectrum at 360 K, as a reference location for the UTLS.

The age spectra of air from the NH extratropics, SH extratropics, and tropics are illustrated in Fig. 4. The transport seasonality is evident for the NH extratropics and SH extratropics origin air, even stronger than the seasonality for the age spectra with tropical origin, which is consistent with the results based on the AMF (Fig. 1). The first peak of the NH extratropical age spectrum during boreal summer and autumn (Fig. 4g, Fig. 4j and factor 0.1) is a very strong signature compared to the SH extratropical age spectrum during austral summer and autumn (Fig. 4b, Fig. 4e and factor 0.02), which means that much more young air can be expected in the NH compared to the SH. The age spectrum of NH extratropical origin air always shows large PDF values at young transit times during boreal summer, and nearly zero during boreal winter, which suggests that the pollutants from the NH extratropics are being transported to the global UTLS primarily during boreal summer.

Age spectrum and mean AoA from the SH extratropics show a lot of similarities to those from the NH extratropics shifted by 6 months. However, NH extratropical origin young air (< 6 months) shows peak values around the ASM region (Fig. 4g and Fig. 4j). The flushing of the NH lowermost stratosphere with NH extratropical origin air during boreal summer and autumn (JJA and SON) is more pronounced compared to the flushing of the SH lowermost stratosphere with SH extratropical origin air during austral summer and autumn (DJF and MAM). The mean AoA shows that inter-hemispheric transport proceeds faster from the SH extratropics to the NH extratropics than from the NH extratropics to the SH extratropics in qualitative agreement with results found by Konopka et al. (2017, their Fig. 5) related to the weaker barrier along the jet in the NH (see Fig. 3) which

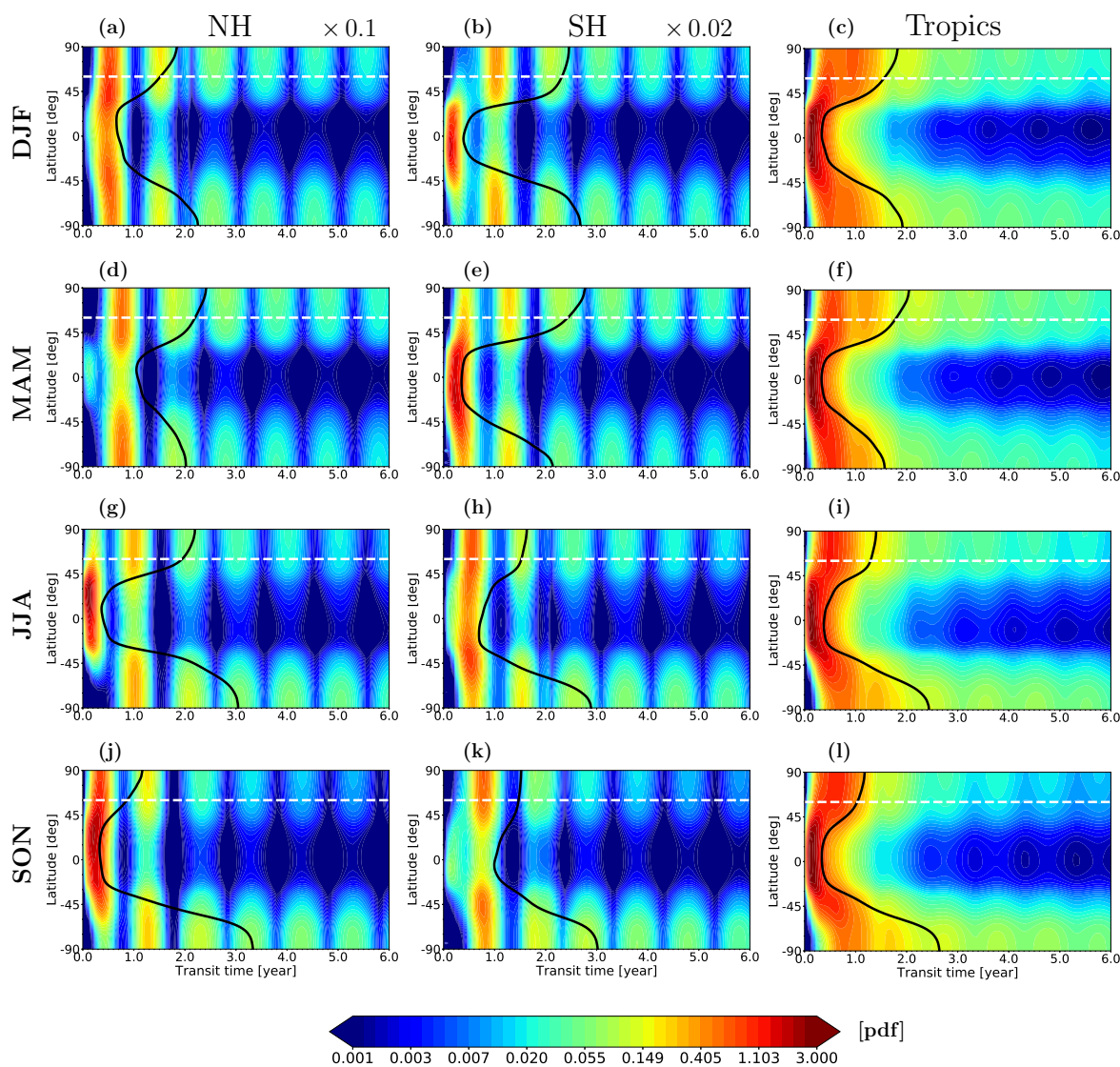


Figure 4. Age spectra as (partial) transit time probability density functions, PDFs, calculated for air originating from three source regions: NH extratropics (30–90° N), SH extratropics (30–90° S), and tropics (30° S–30° N). Age spectra are shown at $\theta = 360$ K (destination region) for all seasons. For each season, the total sum of the integral of the age spectra over all 3 source regions (i.e. over all partial contributions) is ~ 1 , due to our approximation limiting the maximal transit time to 10 years. The thick black line shows the mean AoA as derived from the age spectrum. White dashed line marks the 60° N latitude band. For better comparison, the colorbars of the NH extratropics (0.1) and SH extratropics (0.02) age spectrum are rescaled.



allows faster horizontal transport. Another important asymmetry is that, with exception of MAM, the mean AoA is always older in the SH than in the NH for all other seasons and for all source tracers. This is mainly a consequence of hemispheric differences in the wave-driven eddy mixing, being stronger in the NH throughout the year (Rosenlof, 1995; Konopka et al., 2015).

210 Figure 5 confines the global age spectrum shown in Fig. 4 to partial age spectra at the latitude of 60° N, which defines the spectra from individual source region without normalization to 1. The age spectrum for the NH extratropical origin air (Fig. 5a) shows multiple peaks caused primarily by the interplay between Hadley and BD circulations. As the Hadley cell upwelling is shifted to the NH subtropics during boreal summer, this is the season favoring upward transport from the NH surface, and peaks in the spectrum are related to air originating at the NH surface in early summer. The youngest peak is in JJA at transit times
215 of around 2 months as a result of an "in phase" interaction between the Hadley and the lower branch of the BD circulation. The respective first peaks in the following seasons are shifted accordingly, which suggests that most of air in the NH high latitude region with origin in the NH extratropical boundary layer is emitted during boreal early summer. Although the tropical upwelling has its maximum in boreal winter and spring, it does not significantly transport the NH extratropical origin air to the high latitude lower stratosphere. This is mainly because the Hadley cell supports such transport pathway rather in summer than
220 in winter and spring (Fig. 2). In addition, transport of the NH extratropical origin air to the high latitudes maximizes in boreal autumn. Note that the second peak in JJA resulting from the NH extratropical origin air is higher than the first peak. The mean AoA shows youngest value in boreal autumn (SON) and oldest value in boreal spring (MAM).

Although the structure of age spectrum of the SH extratropical origin air (Fig. 5b) also includes multiple peaks like that from NH extratropics, its total contribution is almost 10 times smaller than the respective contribution from the NH extratropics. The
225 first peak in age spectra in each season from MAM to DJF is delayed by around 3 months accordingly, which again suggests that the main contribution from SH extratropics originates in austral summer. The mean AoA from the SH extratropics is older than that from the NH extratropics during each season except in JJA.

The age spectrum of tropical origin (Fig. 5c) shows by far the highest partial contribution (10 and 100 times larger than that of the NH and SH, respectively). Unlike the age spectrum of the NH extratropics and SH extratropics origin air, the tropical
230 age spectrum in JJA and SON has only one clear peak at transit time around 6 months. During DJF and MAM the tropical age spectrum shows more a multimodal shape with primary peak at transit time around 6 months and a secondary peak delayed by a few months. The first peak might be related to the Hadley and BD circulations combining with the rapid isentropic transport. The second peak shows similar transit time as the air originating from the SH extratropics, which suggests that the peak might be driven by recirculation within the shallow branch of the BD circulation. The age spectra along 60° S on the 360 K isentropic
235 surface shows similar patterns with 6 months shift and different amplitudes (not shown).

Finally, to get the global view of the mean transit time seasonality from the three source regions, we calculate for each season the mean AoA from the respective age spectrum using Eq. 2. The mean AoA for each source region and season with and without the annual mean removed are compared in Figure 6. In general, we arrive at a similar view on the well-known seasonality and hemispheric asymmetries of the Hadley and BD circulation (e.g. Konopka et al., 2015, and citations therein).
240 While the seasonality of the tropical upwelling dominates the tropical features, the strength of isentropic poleward transport

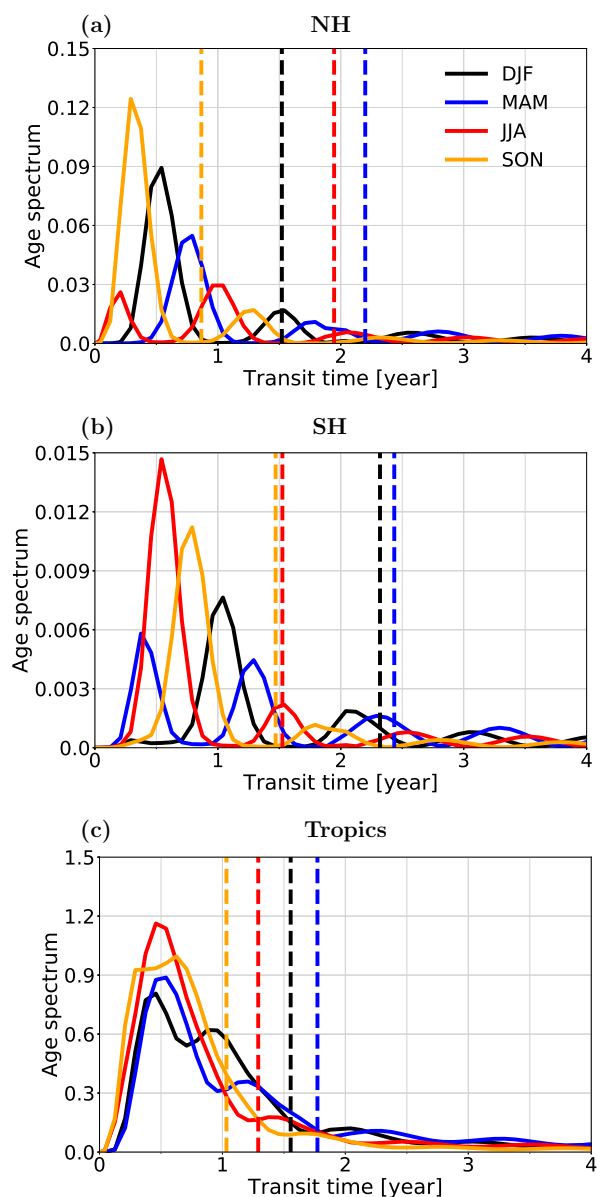


Figure 5. Partial age spectra of the air with the origin in: NH extratropics (a), SH extratropics (b), and tropics (c) calculated at 360 K along 60° N (destination region). Different colours represent different seasons. Vertical dashed lines indicate the mean AoA. Note different ranges of the y-axis (Tropics = 10×NH, NH = 10×SH) which quantify relative differences of the considered source regions.)

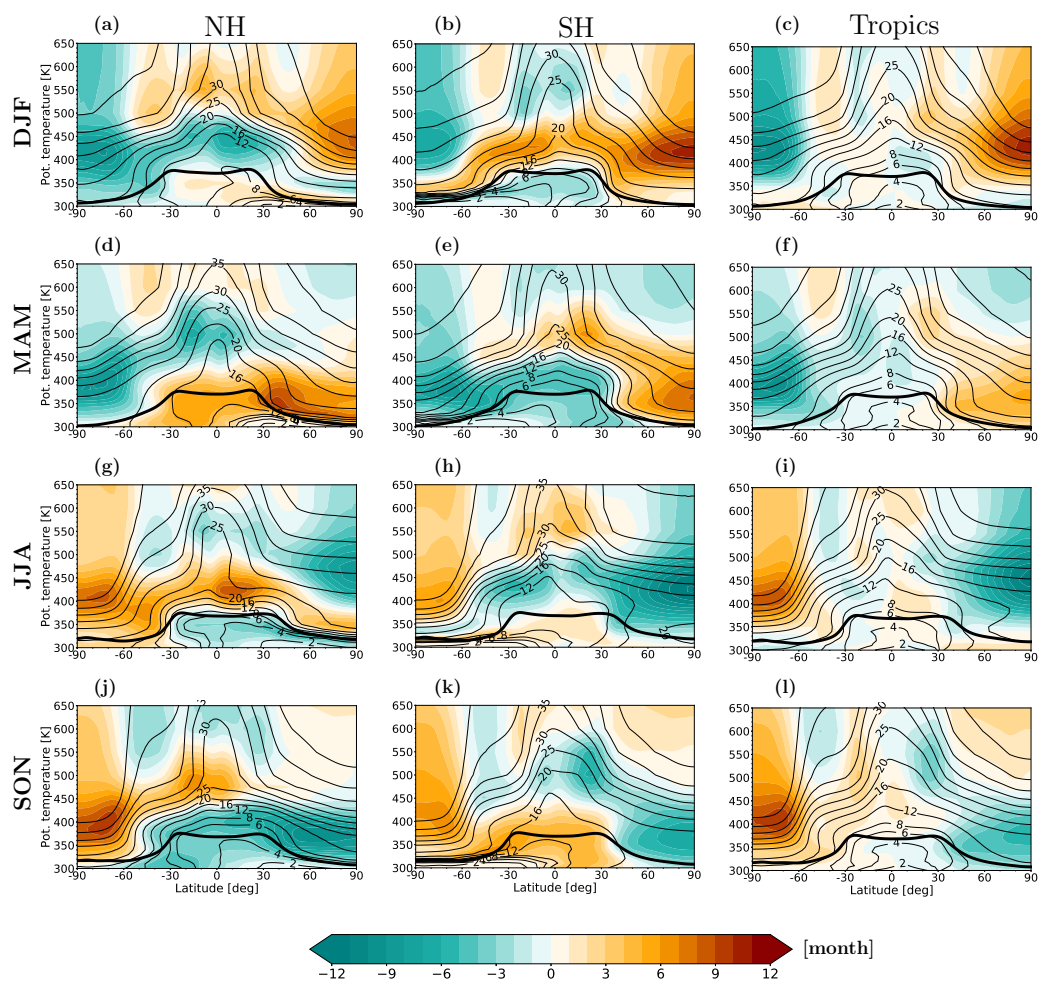


Figure 6. Climatology of the mean age of air (AoA, 1999-2017, black contours) and the AoA anomaly with respect to this climatology (colour shading) from the NH extratropics (30°-90° N, left), SH extratropics (30°-90° S, middle), and tropics (30° S-30° N, right) for DJF (top row), MAM (second row), JJA (third row), and SON (bottom row). The thick black line shows the (WMO) tropopause.



and polar vortices explain the patterns at high latitudes. The highest amplitude in the AoA anomalies for NH sources can be diagnosed in the polar SH and vice versa for the SH sources in the polar NH. The amplitude of seasonality in the tropics, especially of the air originating in the tropics, is much smaller compared to that in the NH extratropics and SH extratropics.

The tropospheric air originating from the NH extratropics shows younger mean AoA during boreal summer (JJA) mainly
245 in the NH (negative anomalies in Fig. 6g) leading to the flushing with fresh air and the propagation of young air upward and southward to the global stratosphere in the following season. Mean AoA patterns from the SH extratropics show a lot of similarities to those from the NH extratropics with a 6 months shift. The young tropospheric air originating from the SH extratropics starts filling the UTLS from austral summer (DJF) in the SH and is transported upwards and northwards in the following seasons. Besides the similarities, SH extratropical origin air shows an old layer (about 20 months) around the
250 NH extratropical tropopause (around the altitude range of 320-350 K) during JJA (Fig. 6h) linked to the flushing of the NH lowermost stratosphere with NH extratropical air (Fig. 1g), this old layer also exists in the distribution of tropical origin air over high latitude regions (Fig. 6i).

Beyond these known features, some interesting asymmetries of the cross-hemispheric transport can be diagnosed. Comparing the left and middle column of Fig. 6, we found that the age of SH extratropical origin air in the NH is younger than the age of
255 NH extratropical origin air in the SH associated with the fast flushing of the NH lower and middle stratosphere with young air in summer (Hegglin and Shepherd, 2007; Bönisch et al., 2009; Orbe et al., 2016; Konopka et al., 2017). The latitudinal mean AoA gradients in the tropical upper troposphere are weak because of the increased latitudinal transport caused by the upper branch of the Hadley circulation and isentropic mixing. The latitudinal mean AoA gradients of NH extratropical tracer in the SH during JJA are larger than those of SH extratropical tracer in the NH during DJF caused by the stronger barrier along the
260 jet in the SH during austral winter.

4 Pathways of inter-hemispheric transport

In Sect. 3, we discussed the transport from the three source regions based on zonal mean results. Clear hemispheric asymmetry features of transport were noticed in AMF and age spectra. The transit time from the SH extratropical surface to the NH is shorter than that from the NH extratropical surface to the SH. The contributions (AMF) of the NH extratropical air to the global
265 UTLS are around 5 times larger than those from the SH associated with the stronger monsoons and weaker transport barriers in the NH during boreal summer, which allow strong meridional and inter-hemispheric transport. To gain deeper insights into these hemispheric asymmetries in transport, we disentangle the transport pathways in this section using zonally resolved data. Since most of the anthropogenic pollutants are emitted in the NH and the contributions from the NH extratropics to the SH are much larger than vice versa, the transport pathways from the NH to the SH are of our particular interest.

The monthly evolution of young air (AoA less than 3 months) from the NH extratropics along the latitude of 10° S longitude-pressure cross-section is illustrated in Fig. 7. We choose 10° S to reduce the influence of reversible transport across the equator. The AMF from January to May is nearly zero and therefore only May is shown (Fig. 7a). First significant signatures become
270 evident in June–July, maximize in August–September, and vanish in November. There is almost no inter-hemispheric ex-

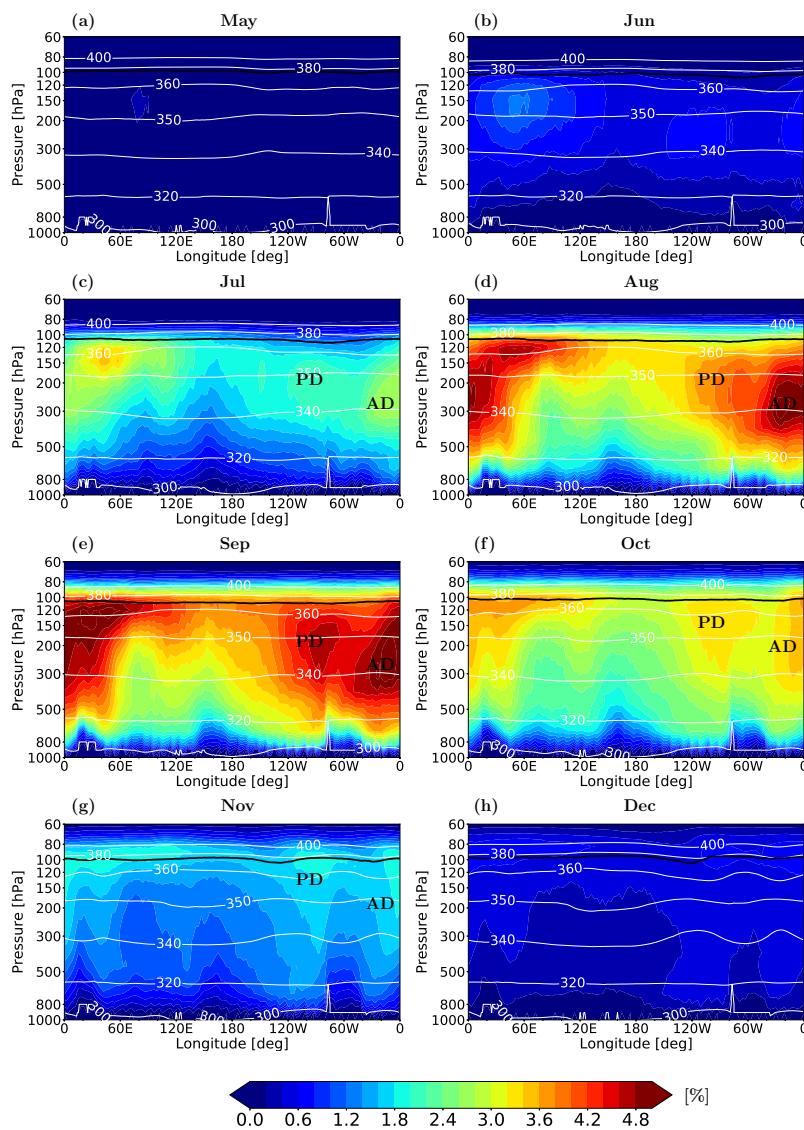


Figure 7. Longitude-pressure cross-section along the latitude of 10° S of monthly mean NH extratropical young (< 3 months) AMF (colour shading) during 1999-2017. White lines show isentropic levels, the thick black line the (WMO) tropopause. PD and AD respectively indicate the rough locations of the Pacific westerly ducts and the Atlantic westerly ducts.

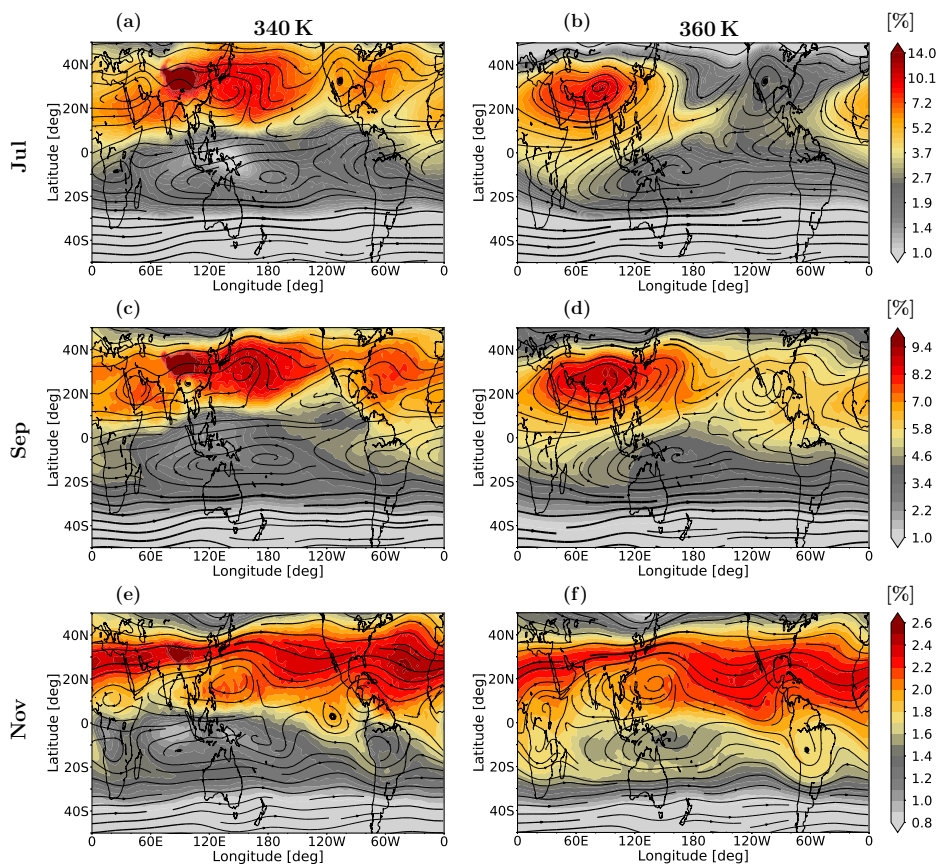


Figure 8. A snapshot of the horizontal distribution of the NH extratropical origin young (< 3 months) air on the 340 K and 360 K isentropic surface during July, September, and November. Streamlines show horizontal winds.

change in the lower troposphere, probably related to stable easterlies, which are less disturbed by Kelvin waves and which
275 effectively act as a meridional transport barrier (see winds in Fig. 3).

Most of the young air masses from the NH extratropics are transported to the SH between 0 and 120° E (ASM region)
from June to October (Fig. 7b-f), with a maximum around $\theta = 360$ K, which suggests a dominant role of ASM in the inter-
hemispheric transport in agreement with the findings from Orbe et al. (2016). The cross hemispheric transport over the At-
lantic (around 20° W) and Pacific (around 80° W) happens at lower altitudes between 340 and 350 K compared to the cross-
280 hemispheric transport between about 0-120° E over ASM region. To disentangle which flow properties in the NH cause this
pattern of inter-hemispheric exchange, a zonally revolved view of both the AMF (less than 3 months) and the zonal wind over-
plotted with PV contours is shown in Fig. 8 and Fig. 9, respectively. Here, monthly means (July, September, and November) of
young AMF are plotted at 340 and 360 K potential temperature levels.



Figure 8 shows that the time evolution of the AMF crossing the equator is caused by the combination of two dynamical
285 processes: ASM anticyclonic flow and related eddy shedding, mainly at $\theta = 360$ K (Popovic and Plumb, 2001; Orbe et al.,
2016) and the eastward-propagating Rossby wave dynamics across the equator in regions of westerly winds (westerly ducts),
mainly over the Pacific and the Atlantic. In July, the peak of the young air (less than 3 months) at 340 K is located over Tibetan
plateau and is related to the elevated orography over Tibet which is very close to the 340 K level, so the peak is strongly affected
by the released boundary tracers. A second peak is located in the subtropics of Western Pacific and can be attributed to the
290 outflow from monsoon circulations at lower level. The ASM circulation keeps supplying the NH extratropical young air from
lower level (Fig. 8a and Fig. 8c) and isolates most of the young air inside the center of the ASM anticyclone at 360 K (Fig. 8b
and Fig. 8d) during July–September. Part of the NH extratropical origin air which was entrained into the ASM anticyclone
moves southward and westward along with the ASM circulation, and is then transported to the SH by eddy shedding detaching
ASM air from the anticyclone and subsequently being transported into the SH (Popovic and Plumb, 2001; Orbe et al., 2016)
295 and to the Atlantic by the easterly flow on the southern edge of the ASM anticyclone.

The westerly ducts can be clearly seen in the respective climatology of the zonal wind and PV shown in Fig. 9. The tongues
of PV and the related anomalies of the westerly wind can be diagnosed in the NH, both over the Pacific and the Atlantic, from
July to November at both potential temperature levels 340 and 360 K. Note that the westerlies in the NH become stronger
from July to November. The impact of the westerly ducts on the cross-hemispheric transport can be deduced from the time
300 evolution of the AMF at 340 K (Fig. 8 left) with some distinct signatures over the Atlantic (July–November) and slightly
weaker signatures over the Pacific (November).

The picture changes at $\theta = 360$ K (Fig. 8 right). While the eddy shedding mechanism plays an important role from July to
September, there is only weak transport from the NH to the tropics and to the SH through the westerly ducts during this time.
This implies the important role of the ASM circulation in the asymmetry of inter-hemispheric transport at the 360 K level.
305 However, starting from September, the westerly ducts start to drive the cross-hemispheric transport (Fig. 8d and Fig. 8f). On
the one hand, the westerly ducts are getting stronger in boreal autumn and winter (Fig. 9d and Fig. 9f) compared to boreal
summer (Fig. 9b). On the other hand, most of the tracers transported across the equator through the westerly ducts originates
from ASM regions following the evolution of the ASM anticyclone. This suggests that the westerly ducts alone would not
transport a substantial amount of young air masses from the NH extratropics to the SH. It is the interplay between the ASM
310 anticyclone and the westerly ducts which drives the inter-hemispheric transport from boreal summer to fall.

5 Discussion

The air contributions and age spectrum (or AoA) from different source regions to the destination regions in the atmosphere
provide valuable information for understanding the effect of natural and anthropogenic emissions on the atmospheric compo-
sition and climate. However, recent studies show substantial transport uncertainties depending on the used methods, models,
315 and meteorological reanalyses (e.g. Krol et al., 2018; Ploeger et al., 2019).

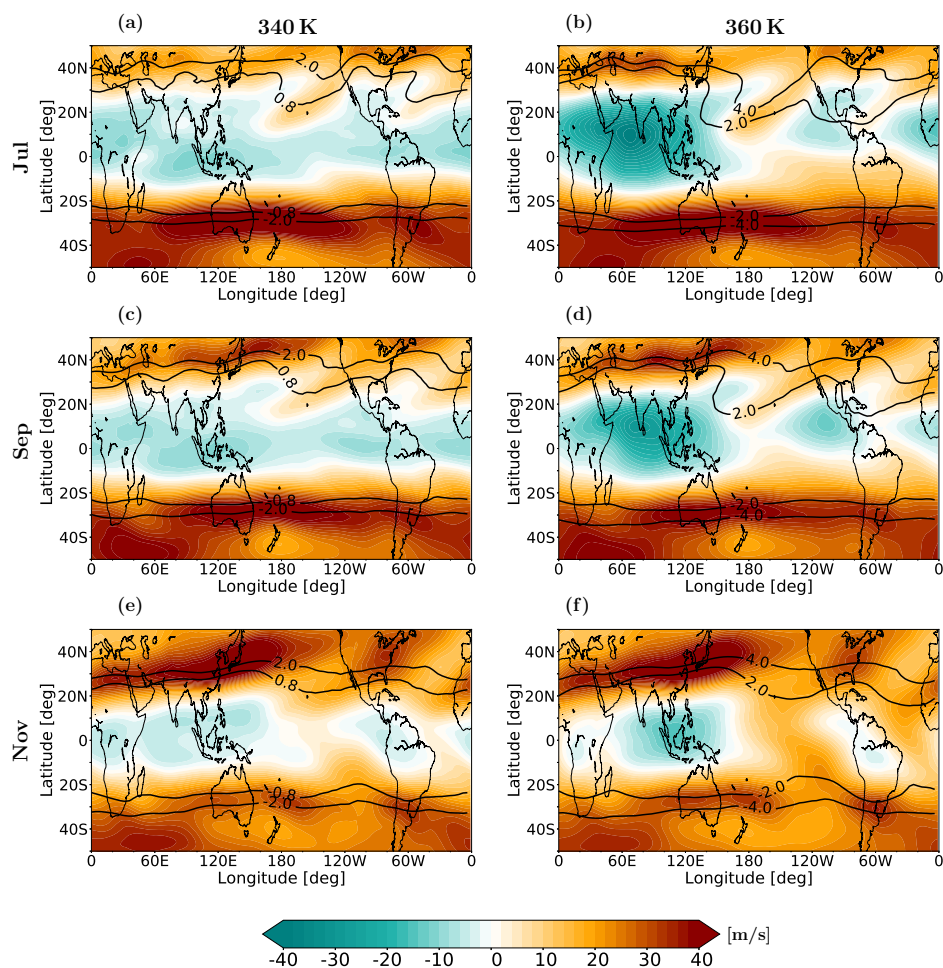


Figure 9. Climatological (1999-2017) horizontal distribution of zonal wind on the 340 K and 360 K isentropic surface during July, September, and November. The potential vorticity is indicated by the black contours.



Recently, Hauck et al. (2020) estimated the age spectra and AMF also using simulations from CLaMS but with the pulse tracers released from the tropopause level over the NH extratropics (30-90° N), SH extratropics (30-90° S), and tropics (30° S-30° N). The first obvious difference to our results is that the NH extratropics and SH extratropics origin air pulsed in the boundary layer contributes much less to the lower stratosphere compared to air originating at tropopause level (Hauck et al., 2020, their Fig. 2). However, the tracers pulsed at the tropopause level are more latitudinally confined compared to the results here. Furthermore, the inter-hemispheric transport is more symmetric and nearly negligible based on the pulse tracers from the tropopause, while the tracers pulsed from the boundary layer show substantial inter-hemispheric transport, especially from the NH extratropics to the SH. This is presumable because the hemispheric differences in transport mainly result from the hemispheric asymmetry of the upward motion of the Hadley circulation in boreal and austral summer, of the land-sea distribution, and of the orography, whose importance decreases with altitude. Note that the strongest cross-hemispheric transport from the NH extratropics to the SH was diagnosed here below the tropopause at potential temperature levels 340 and 360 K. As recently discussed in Yan et al. (2019), the Asian and North American summer monsoon tracers released at lower level (350-360 K) and upper level (370-380 K) show similar results with upper level tracers being more confined in the NH and with lower level tracers significantly crossing the equator.

The age spectra with respect to NH extratropical tropopause in the high latitude lower stratosphere (Hauck et al., 2020, their Fig. 3) show a less distinct multimodal shape with much weaker seasonality compared to spectra with respect to the NH extratropical boundary layer which are strongly affected by the seasonal variation (Fig. 5a). The age spectra for the NH extratropical boundary origin at 60° N on the 360 K surface peak at about 2 months larger transit times compared to age spectra related to the tropopause due to the extra vertical transport from the boundary layer to the tropopause. Both the NH extratropical boundary air and the NH extratropical tropopause air in the NH high latitude lower stratosphere originates at the respective surface in early summer.

Simulations from a two-box model show that the transit time of the NH origin air to the SH is shorter than vice versa associated with the different strength of the seasonal cycle and the asymmetric position of the intertropical convergence zone (Chen et al., 2017; Krol et al., 2018). However, our simulations based on three source domains show that the mean AoA from the NH extratropics surface to the SH is longer than vice versa (Fig. 6). The discrepancy is mainly caused by different definitions of the domains, which are 30-90° N and 30-90° S in our study, while Chen et al. (2017) and Krol et al. (2018) define the whole hemisphere to represent the NH and SH.

6 Conclusions

This paper presents air mass fractions and age spectra with respect to the different surface patches: NH extratropics (30-90° N), SH extratropics (30-90° S), and tropics (30° S-30° N) source regions. The CLaMS model is used for carrying out simulations covering the period 1989-2017. We find that air originating at the NH extratropical surface shows about five times larger amounts in the UTLS compared to air from the SH surface. Although the tropical origin air dominates the atmosphere, the amplitude of seasonal variation is comparable for transport from the tropics and from the NH extratropics.



Both the SH extratropics and NH extratropics age spectra show more pronounced seasonality compared to the seasonality
350 of tropical age spectra. We notice that the air in the northern high latitude regions originating from the NH extratropics is
mainly transported into the UTLS from early summer to fall, rendering this season particularly important for transport of
anthropogenic pollutants into high latitude regions. The transit time of NH extratropical origin air to the SH extratropics is
longer than vice versa, although the ASM helps to reduce this transit time.

Further analyses suggest that the cross-hemispheric transport of fresh air (AoA less than 3 months) from the NH extratropics
355 to the SH mainly occurs in the altitude range of 320-400 K. The ASM circulation has been recognized as an important driver
for cross hemispheric transport in simulations (e.g. Orbe et al., 2016) and observations, i.e. aerosol data from wildfire plume
(e.g. Kloss et al., 2019) and volcanic plume (e.g. Wu et al., 2017). The westerly ducts have been reported as another driver
of inter-hemispheric transport (e.g. Webster and Holton, 1982; Tomas and Webster, 1994). In agreement with these previous
studies, we find crucial roles of the ASM circulation and the westerly ducts in causing the cross equatorial transport. However,
360 it is neither the ASM circulation nor the westerly ducts alone, but the interplay between ASM and westerly ducts that matters
for the inter-hemispheric transport. In particular, it is not the region of strongest westerly ducts (Pacific) which allows the
strongest transport but the Atlantic region, where the westerlies are weaker, but which is closer to the ASM, coupling with the
ASM and causing strongest cross-equatorial transport.

Data availability. The CLaMS model outputs may be obtained from the authors upon request.

365 *Author contributions.* XY analyzed the data. FP carried out the model simulations. PK and FP contributed to the design of the analysis. MH
contributed codes for the analysis. PK, FP, MH, AP provided helpful discussions and comments. XY wrote the paper with contributions from
all co-authors.

Competing interests. The authors declare that they have no conflict of interest.

Acknowledgements. We thank the ECMWF for providing ERA-Interim meteorological reanalysis data for this study. We gratefully ac-
370 knowledge the computing time for the CLaMS simulations granted through VSR project ID JICG11 on the supercomputer JURECA at
Forschungszentrum Jülich. This research has been supported by the National Natural Science Foundation of China project (grant nos.
41905040, 91837311, and 91937302), National Key Research and Development Program of China (grant no. 2018YFC1505703), and a joint
DFG-NSFC research project (DFG grant no. 392169209 and NSFC grant no. 20171352419). Felix Ploeger was funded by the Helmholtz
Association under grant no. VH-NG-1128 (Helmholtz Young Investigators Group A-SPECi).



375 References

- Bönisch, H., Engel, A., Curtius, J., Birner, T., and Hoor, P.: Quantifying transport into the lowermost stratosphere using simultaneous in-situ measurements of SF₆ and CO₂, *Atmospheric Chemistry and Physics*, 9, 5905–5919, <https://doi.org/10.5194/acp-9-5905-2009>, 2009.
- Bowman, K. P.: Transport of carbon monoxide from the tropics to the extratropics, *Journal of Geophysical Research: Atmospheres*, 111, <https://doi.org/10.1029/2005JD006137>, 2006.
- 380 Bowman, K. P. and Carrie, G. D.: The Mean-Meridional Transport Circulation of the Troposphere in an Idealized GCM, *Journal of the Atmospheric Sciences*, 59, 1502–1514, [https://doi.org/10.1175/1520-0469\(2002\)059<1502:TMMTCO>2.0.CO;2](https://doi.org/10.1175/1520-0469(2002)059<1502:TMMTCO>2.0.CO;2), 2002.
- Bowman, K. P. and Cohen, P. J.: Interhemispheric Exchange by Seasonal Modulation of the Hadley Circulation, *Journal of the Atmospheric Sciences*, 54, 2045–2059, [https://doi.org/10.1175/1520-0469\(1997\)054<2045:IEBSMO>2.0.CO;2](https://doi.org/10.1175/1520-0469(1997)054<2045:IEBSMO>2.0.CO;2), 1997.
- Butchart, N.: The Brewer-Dobson circulation, *Rev. Geophys.*, 52, 157–184, <https://doi.org/10.1002/2013RG000448>, 2014.
- 385 Chen, G., Orbe, C., and Waugh, D.: The role of monsoon-like zonally asymmetric heating in interhemispheric transport, *Journal of Geophysical Research: Atmospheres*, 122, 3282–3298, <https://doi.org/10.1002/2016JD026427>, 2017.
- Czeplak, G. and Junge, C.: Studies of Interhemispheric Exchange in the Troposphere by a Diffusion Model, in: *International Union of Theoretical and Applied Mechanics and International Union of Geodesy and Geophysics*, edited by Frenkiel, F. and Munn, R., vol. 18 of *Advances in Geophysics*, pp. 57 – 72, Elsevier, [https://doi.org/10.1016/S0065-2687\(08\)60571-3](https://doi.org/10.1016/S0065-2687(08)60571-3), 1975.
- 390 Dee, D. P., Uppala, S. M., Simmons, A. J., Berrisford, P., Poli, P., Kobayashi, S., Andrae, U., Balmaseda, M. A., Balsamo, G., Bauer, P., Bechtold, P., Beljaars, A. C. M., van de Berg, L., Bidlot, J., Bormann, N., Delsol, C., Dragani, R., Fuentes, M., Geer, A. J., Haimberger, L., Healy, S. B., Hersbach, H., Holm, E. V., Isaksen, I., Kallberg, P., Köhler, M., Matricardi, M., McNally, A. P., Monge-Sanz, B. M., Morcrette, J.-J., Park, B.-K., Peubey, C., de Rosnay, P., Tavolato, C., Thepaut, J.-N., and Vitart, F.: The ERA-Interim reanalysis: configuration and performance of the data assimilation system, *Q. J. R. Meteorol. Soc.*, 137, 553–597, <https://doi.org/10.1002/qj.828>, 2011.
- 395 Denning, A. S., Holzer, M., Gurney, K. R., Heimann, M., Law, R. M., Rayner, P. J., Fung, I. Y., Fan, S.-M., Taguchi, S., Friedlingstein, P., Balkanski, Y., Taylor, J., Maiss, M., and Levin, I.: Three-dimensional transport and concentration of SF₆ A model intercomparison study (TransCom 2), *Tellus B: Chemical and Physical Meteorology*, 51, 266–297, <https://doi.org/10.3402/tellusb.v51i2.16286>, 1999.
- Dlugokencky, E. J., Bruhwiler, L., White, J. W. C., Emmons, L. K., Novelli, P. C., Montzka, S. A., Masarie, K. A., Lang, P. M., Crotwell, A. M., Miller, J. B., and Gatti, L. V.: Observational constraints on recent increases in the atmospheric CH₄ burden, *Geophysical Research*
- 400 *Letters*, 36, <https://doi.org/10.1029/2009GL039780>, 2009.
- Engel, A., Möbius, T., Bönisch, H., Schmidt, U., Heinz, R., Levin, I., Atlas, E., Aoki, S., Nakazawa, T., Sugawara, S., Moore, F., Hurst, D., Elkins, J., Schauffler, S., Andrews, A., and Boering, K.: Age of stratospheric air unchanged within uncertainties over the past 30 years, *Nature Geoscience*, 2, 28–31, <https://doi.org/10.1038/ngeo388>, 2009.
- Engel, A., Bönisch, H., Ullrich, M., Sitals, R., Membrive, O., Danis, F., and Crevoisier, C.: Mean age of stratospheric air derived from AirCore observations, *Atmospheric Chemistry and Physics*, 17, 6825–6838, <https://doi.org/10.5194/acp-17-6825-2017>, <https://www.atmos-chem-phys.net/17/6825/2017/>, 2017.
- Erukhimova, T. and Bowman, K. P.: Role of convection in global-scale transport in the troposphere, *Journal of Geophysical Research: Atmospheres*, 111, <https://doi.org/10.1029/2005JD006006>, 2006.
- Francey, R. J. and Frederiksen, J. S.: The 2009–2010 step in atmospheric CO₂ interhemispheric difference, *Biogeosciences*, 13, 873–885, <https://doi.org/10.5194/bg-13-873-2016>, 2016.
- 410



- Fritsch, F., Garny, H., Engel, A., Bönisch, H., and Eichinger, R.: Sensitivity of Age of Air Trends on the derivation method for non-linear increasing tracers, *Atmospheric Chemistry and Physics Discussions*, 2019, 1–23, <https://doi.org/10.5194/acp-2019-974>, <https://www.atmos-chem-phys-discuss.net/acp-2019-974/>, 2019.
- 415 Fueglistaler, S., Wernli, H., and Peter, T.: Tropical troposphere-to-stratosphere transport inferred from trajectory calculations, *J. Geophys. Res.*, 109, D03108, <https://doi.org/10.1029/2003JD004069>, 2004.
- Fueglistaler, S., Dessler, A. E., Dunkerton, T. J., Folkins, I., Fu, Q., and Mote, P. W.: Tropical tropopause layer, *Rev. Geophys.*, 47, RG1004, <https://doi.org/10.1029/2008RG000267>, 2009.
- Garny, H., Birner, T., Bönisch, H., and Bunzel, F.: The effects of mixing on Age of Air, *J. Geophys. Res.*, 119, <https://doi.org/10.1002/2013JD021417>, 2014.
- 420 Gloor, M., Dlugokencky, E., Brenninkmeijer, C., Horowitz, L., Hurst, D. F., Dutton, G., Crevoisier, C., Machida, T., and Tans, P.: Three-dimensional SF₆ data and tropospheric transport simulations: Signals, modeling accuracy, and implications for inverse modeling, *Journal of Geophysical Research: Atmospheres*, 112, <https://doi.org/10.1029/2006JD007973>, 2007.
- Hall, T. M. and Plumb, R. A.: Age as a diagnostic of stratospheric transport, *J. Geophys. Res.*, 99, 1059–1070, 1994.
- Hartley, D. E. and Black, R. X.: Mechanistic analysis of interhemispheric transport, *Geophysical Research Letters*, 22, 2945–2948, <https://doi.org/10.1029/95GL02823>, 1995.
- 425 Hauck, M., Fritsch, F., Garny, H., and Engel, A.: Deriving stratospheric age of air spectra using an idealized set of chemically active trace gases, *Atmospheric Chemistry and Physics*, 19, 5269–5291, <https://doi.org/10.5194/acp-19-5269-2019>, <https://www.atmos-chem-phys.net/19/5269/2019/>, 2019.
- Hauck, M., Bönisch, H., Hoor, P., Keber, T., Ploeger, F., Schuck, T. J., and Engel, A.: A convolution of observational and model data to estimate age of air spectra in the northern hemispheric lower stratosphere, *Atmospheric Chemistry and Physics*, 20, 8763–8785, <https://doi.org/10.5194/acp-20-8763-2020>, 2020.
- 430 Hegglin, M. I. and Shepherd, T. G.: O₃-N₂O correlations from the Atmospheric Chemistry Experiment: Revisiting a diagnostic of transport and chemistry in the stratosphere, *J. Geophys. Res.*, D19301, <https://doi.org/10.1029/2006JD008281>, 2007.
- Holton, J. R., Haynes, P., McIntyre, M. E., Douglass, A. R., Rood, R. B., and Pfister, L.: Stratosphere-troposphere exchange, *Rev. Geophys.*, 33, 403–439, 1995.
- 435 Hoor, P., Fischer, H., and Lelieveld, J.: Tropical and extratropical tropospheric air in the lowermost stratosphere over Europe: A CO-based budget, *Geophysical Research Letters*, 32, <https://doi.org/10.1029/2004GL022018>, 2005.
- Hoskins, B. J., McIntyre, M. E., and Robertson, A. W.: On the use and significance of isentropic potential vorticity maps, *Q. J. R. Meteorol. Soc.*, 111, 877–946, 1985.
- 440 Jacob, D. J., Prather, M. J., Wofsy, S. C., and McElroy, M. B.: Atmospheric distribution of ⁸⁵Kr simulated with a general circulation model, *Journal of Geophysical Research: Atmospheres*, 92, 6614–6626, <https://doi.org/10.1029/JD092iD06p06614>, 1987.
- Kloss, C., Berthet, G., Sellitto, P., Ploeger, F., Bucci, S., Khaykin, S., Jégou, F., Taha, G., Thomason, L. W., Barret, B., Le Flochmoen, E., von Hobe, M., Bossolasco, A., Bègue, N., and Legras, B.: Transport of the 2017 Canadian wildfire plume to the tropics via the Asian monsoon circulation, *Atmospheric Chemistry and Physics*, 19, 13 547–13 567, <https://doi.org/10.5194/acp-19-13547-2019>, 2019.
- 445 Konopka, P., Steinhorst, H.-M., Groß, J.-U., Günther, G., Müller, R., Elkins, J. W., Jost, H.-J., Richard, E., Schmidt, U., Toon, G., and McKenna, D. S.: Mixing and Ozone Loss in the 1999–2000 Arctic Vortex: Simulations with the 3-dimensional Chemical Lagrangian Model of the Stratosphere (CLaMS), *J. Geophys. Res.*, 109, D02315, <https://doi.org/10.1029/2003JD003792>, 2004.



- Konopka, P., Ploeger, F., Tao, M., Birner, T., and Riese, M.: Hemispheric asymmetries and seasonality of mean age of air in the lower stratosphere: Deep versus shallow branch of the Brewer-Dobson circulation, *J. Geophys. Res.*, 120, 2053–2066, <https://doi.org/10.1002/2014JD022429>, 2015.
- Konopka, P., Ploeger, F., Tao, M., and Riese, M.: Regionally Resolved Diagnostic of Transport: A Simplified Forward Model for CO₂, *Journal of the Atmospheric Sciences*, 74, 2689–2700, <https://doi.org/10.1175/JAS-D-16-0367.1>, 2017.
- Kovács, T., Feng, W., Totterdill, A., Plane, J. M. C., Dhomse, S., Gómez-Martín, J. C., Stiller, G. P., Haenel, F. J., Smith, C., Forster, P. M., García, R. R., Marsh, D. R., and Chipperfield, M. P.: Determination of the atmospheric lifetime and global warming potential of sulfur hexafluoride using a three-dimensional model, *Atmospheric Chemistry and Physics*, 17, 883–898, <https://doi.org/10.5194/acp-17-883-2017>, 2017.
- Krol, M., de Bruine, M., Killaars, L., Ouwersloot, H., Pozzer, A., Yin, Y., Chevallier, F., Bousquet, P., Patra, P., Belikov, D., Maksyutov, S., Dhomse, S., Feng, W., and Chipperfield, M. P.: Age of air as a diagnostic for transport timescales in global models, *Geoscientific Model Development*, 11, 3109–3130, <https://doi.org/10.5194/gmd-11-3109-2018>, <https://www.geosci-model-dev.net/11/3109/2018/>, 2018.
- Kunz, A., Konopka, P., Müller, R., and Pan, L. L.: Dynamical tropopause based on isentropic potential vorticity gradients, *J. Geophys. Res.*, 116, D01110, <https://doi.org/10.1029/2010JD014343>, warning: BibtextKey has changed!!, 2011.
- Levine, J. G., Braesicke, P., Harris, N. R. P., Savage, N. S., and Pyle, J. A.: Pathways and timescales for troposphere-to-stratosphere transport via the tropical layer and their relevance for very short-lived substances, *J. Geophys. Res.*, 112, D04308, <https://doi.org/10.1029/2005JD006940>, 2007.
- Liang, Q., Newman, P. A., Daniel, J. S., Reimann, S., Hall, B. D., Dutton, G., and Kuijpers, L. J. M.: Constraining the carbon tetrachloride (CCl₄) budget using its global trend and inter-hemispheric gradient, *Geophysical Research Letters*, 41, 5307–5315, <https://doi.org/10.1002/2014GL060754>, 2014.
- Lintner, B. R., Gilliland, A. B., and Fung, I. Y.: Mechanisms of convection-induced modulation of passive tracer interhemispheric transport interannual variability, *Journal of Geophysical Research: Atmospheres*, 109, <https://doi.org/10.1029/2003JD004306>, 2004.
- Maiss, M., Steele, L., Francey, R. J., Fraser, P. J., Langenfelds, R. L., Trivett, N. B., and Levin, I.: Sulfur hexafluoride—A powerful new atmospheric tracer, *Atmospheric Environment*, 30, 1621 – 1629, [https://doi.org/https://doi.org/10.1016/1352-2310\(95\)00425-4](https://doi.org/https://doi.org/10.1016/1352-2310(95)00425-4), joint 8th CAGCP and 2nd IGAC Conference on Global Atmospheric Chemistry, 1996.
- McKenna, D. S., Konopka, P., Grooß, J.-U., Günther, G., Müller, R., Spang, R., Offermann, D., and Orsolini, Y.: A new Chemical Lagrangian Model of the Stratosphere (CLaMS): 1. Formulation of advection and mixing, *J. Geophys. Res.*, 107, 4309, <https://doi.org/10.1029/2000JD000114>, 2002.
- Müller, J.-F. and Brasseur, G.: IMAGES: A three-dimensional chemical transport model of the global troposphere, *Journal of Geophysical Research: Atmospheres*, 100, 16 445–16 490, <https://doi.org/10.1029/94JD03254>, 1995.
- Naus, S., Montzka, S. A., Pandey, S., Basu, S., Dlugokencky, E. J., and Krol, M.: Constraints and biases in a tropospheric two-box model of OH, *Atmospheric Chemistry and Physics*, 19, 407–424, <https://doi.org/10.5194/acp-19-407-2019>, <https://www.atmos-chem-phys.net/19/407/2019/>, 2019.
- Orbe, C., Waugh, D. W., Newman, P. A., and Steenrod, S.: The Transit-Time Distribution from the Northern Hemisphere Midlatitude Surface, *Journal of the Atmospheric Sciences*, 73, 3785–3802, <https://doi.org/10.1175/JAS-D-15-0289.1>, 2016.
- Orbe, C., Yang, H., Waugh, D. W., Zeng, G., Morgenstern, O., Kinnison, D. E., Lamarque, J.-F., Tilmes, S., Plummer, D. A., Scinocca, J. F., Josse, B., Marecal, V., Jöckel, P., Oman, L. D., Strahan, S. E., Deushi, M., Tanaka, T. Y., Yoshida, K., Akiyoshi, H., Yamashita, Y., Stenke, A., Revell, L., Sukhodolov, T., Rozanov, E., Pitari, G., Visioni, D., Stone, K. A., Schofield, R., and Banerjee, A.: Large-



- scale tropospheric transport in the Chemistry–Climate Model Initiative (CCMI) simulations, *Atmospheric Chemistry and Physics*, 18, 7217–7235, <https://doi.org/10.5194/acp-18-7217-2018>, <https://www.atmos-chem-phys.net/18/7217/2018/>, 2018.
- Pandey, S., Houweling, S., Krol, M., Aben, I., Monteil, G., Nechita-Banda, N., Dlugokencky, E., Detmers, R., Hasekamp, O., Xu, X., Riley, W., Poulter, B., Zhang, Z., McDonald, K., White, J., Bousquet, P., and Röckmann, T.: Enhanced methane emissions from tropical wetlands during the 2011 la Niña, *Scientific Reports*, 7, <https://doi.org/10.1038/srep45759>, 2017.
- 490 Patra, P. K., Takigawa, M., Dutton, G. S., Uhse, K., Ishijima, K., Lintner, B. R., Miyazaki, K., and Elkins, J. W.: Transport mechanisms for synoptic, seasonal and interannual SF₆ variations and "age" of air in troposphere, *Atmospheric Chemistry and Physics*, 9, 1209–1225, <https://doi.org/10.5194/acp-9-1209-2009>, 2009.
- Patra, P. K., Houweling, S., Krol, M., Bousquet, P., Belikov, D., Bergmann, D., Bian, H., Cameron-Smith, P., Chipperfield, M. P., Corbin, K., Fortems-Cheiney, A., Fraser, A., Gloor, E., Hess, P., Ito, A., Kawa, S. R., Law, R. M., Loh, Z., Maksyutov, S., Meng, L., Palmer, P. I., Prinn, R. G., Rigby, M., Saito, R., and Wilson, C.: TransCom model simulations of CH₄ and related species: linking transport, surface flux and chemical loss with CH₄ variability in the troposphere and lower stratosphere, *Atmospheric Chemistry and Physics*, 11, 12 813–12 837, <https://doi.org/10.5194/acp-11-12813-2011>, 2011.
- 495 Patra, P. K., Krol, M. C., Montzka, S. A., Arnold, T., Atlas, E. L., Lintner, B. R., Stephens, B. B., Xiang, B., Elkins, J. W., Fraser, P. J., Ghosh, A., Hints, E. J., Hurst, D. F., Ishijima, K., Krümmel, P. B., Miller, B. R., Miyazaki, K., Moore, F. L., Mühle, J., O'Doherty, S., Prinn, R. G., Steele, L. P., Takigawa, M., Wang, H. J., Weiss, R. F., Wofsy, S. C., and Young, D.: Observational evidence for interhemispheric hydroxyl-radical parity, *Nature*, 513, 219–223, <https://doi.org/10.1038/nature13721>, 2014.
- 500 Peters, W., Krol, M. C., Dlugokencky, E. J., Dentener, F. J., Bergamaschi, P., Dutton, G., Velthoven, P. v., Miller, J. B., Bruhwiler, L., and Tans, P. P.: Toward regional-scale modeling using the two-way nested global model TM5: Characterization of transport using SF₆, *Journal of Geophysical Research: Atmospheres*, 109, <https://doi.org/10.1029/2004JD005020>, 2004.
- Ploeger, F. and Birner, T.: Seasonal and inter-annual variability of lower stratospheric age of air spectra, *Atmospheric Chemistry and Physics*, 16, 10 195–10 213, <https://doi.org/10.5194/acp-16-10195-2016>, <https://www.atmos-chem-phys.net/16/10195/2016/>, 2016.
- Ploeger, F., Riese, M., Haenel, F., Konopka, P., Müller, R., and Stiller, G.: Variability of stratospheric mean age of air and of the local effects of residual circulation and eddy mixing, *J. Geophys. Res.*, 120, 716–733, <https://doi.org/10.1002/2014JD022468>, 2015.
- 510 Ploeger, F., Konopka, P., Walker, K., and Riese, M.: Quantifying pollution transport from the Asian monsoon anticyclone into the lower stratosphere, *Atmos. Chem. Phys.*, 16, 7055–7066, <https://doi.org/10.5194/acp-17-7055-2017>, 2017.
- Ploeger, F., Legras, B., Charlesworth, E., Yan, X., Diallo, M., Konopka, P., Birner, T., Tao, M., Engel, A., and Riese, M.: How robust are stratospheric age of air trends from different reanalyses?, *Atmospheric Chemistry and Physics*, 19, 6085–6105, <https://doi.org/10.5194/acp-19-6085-2019>, 2019.
- 515 Podglajen, A. and Ploeger, F.: Retrieving the age of air spectrum from tracers: principle and method, *Atmospheric Chemistry and Physics*, 19, 1767–1783, <https://doi.org/10.5194/acp-19-1767-2019>, 2019.
- Pommrich, R., Müller, R., Groß, J.-U., Konopka, P., Ploeger, F., Vogel, B., Tao, M., Hoppe, C. M., Günther, G., Spelten, N., Hoffmann, L., Pumphrey, H.-C., Viciani, S., D'Amato, F., Volk, C. M., Hoor, P., Schlager, H., and Riese, M.: Tropical troposphere to stratosphere transport of carbon monoxide and long-lived trace species in the Chemical Lagrangian Model of the Stratosphere (CLaMS), *Geoscientific Model Development*, 7, 2895–2916, <https://doi.org/10.5194/gmd-7-2895-2014>, 2014.
- 520 Popovic, J. M. and Plumb, R. A.: Eddy Shedding from the Upper-Tropospheric Asian Monsoon Anticyclone, *Journal of the Atmospheric Sciences*, 58, 93–104, [https://doi.org/10.1175/1520-0469\(2001\)058<0093:ESFTUT>2.0.CO;2](https://doi.org/10.1175/1520-0469(2001)058<0093:ESFTUT>2.0.CO;2), 2001.



- Poshyvailo, L., Müller, R., Konopka, P., Günther, G., Riese, M., Podglajen, A., and Ploeger, F.: Sensitivities of modelled water vapour in the lower stratosphere: temperature uncertainty, effects of horizontal transport and small-scale mixing, *Atmospheric Chemistry and Physics*, 18, 8505–8527, 2018.
- Randel, W. J., Moyer, E., Park, M., Jensen, E., Bernath, P., Walker, K., and Boone, C.: Global variations of HDO and HDO/H₂O ratios in the upper troposphere and lower stratosphere derived from ACE–FTS satellite measurements, *J. Geophys. Res.*, 117, D06303, <https://doi.org/10.1029/2011JD016632>, 2012.
- Ratnam, J. V., Behera, S. K., and Yamagata, T.: Role of Cross-Equatorial Waves in Maintaining Long Periods of Low Convective Activity over Southern Africa, *Journal of the Atmospheric Sciences*, 72, 682–692, <https://doi.org/10.1175/JAS-D-14-0063.1>, 2015.
- Ravishankara, A. R., Solomon, S., Turnipseed, A. A., and Warren, R. F.: Atmospheric Lifetimes of Long-Lived Halogenated Species, *Science*, 259, 194–199, <https://doi.org/10.1126/science.259.5092.194>, 1993.
- Ray, E. A., Moore, F. L., Rosenlof, K. H., Davis, S. M., Sweeney, C., Tans, P., Wang, T., Elkins, J. W., Boenisch, H., Engel, A., Sugawara, S., Nakazawa, T., and Aoki, S.: Improving stratospheric transport trend analysis based on SF₆ and CO₂ measurements, *J. Geophys. Res.*, 119, 14 110–14 128, 2014.
- Rosenlof, K. H.: Seasonal cycle of the residual mean meridional circulation in the stratosphere, *J. Geophys. Res.*, 100, 5173 – 5191, 1995.
- Schoeberl, M. R., Douglass, A. R., Polansky, B., Boone, C., Walker, K. A., and Barnath, P.: Estimation of stratospheric age spectrum from chemical tracers, *J. Geophys. Res.*, 110, D21303, <https://doi.org/10.1029/2005JD006125>, 2005.
- Staudt, A. C., Jacob, D. J., Logan, J. A., Bachiochi, D., Krishnamurti, T. N., and Sachse, G. W.: Continental sources, transoceanic transport, and interhemispheric exchange of carbon monoxide over the Pacific, *Journal of Geophysical Research: Atmospheres*, 106, 32 571–32 589, <https://doi.org/10.1029/2001JD900078>, 2001.
- Stiller, G. P., von Clarmann, T., Haedel, F., Funke, B., Glatthor, N., Grabowski, U., Kellmann, S., Kiefer, M., Linden, A., Lossow, S., and López-Puertas, M.: Observed temporal evolution of global mean age of stratospheric air for the 2002 to 2010 period, *Atmos. Chem. Phys.*, 12, 3311–3331, <https://doi.org/10.5194/acp-12-3311-2012>, <http://www.atmos-chem-phys.net/12/3311/2012/>, 2012.
- Tomas, R. A. and Webster, P. J.: Horizontal and Vertical Structure of Cross-Equatorial Wave Propagation, *Journal of the Atmospheric Sciences*, 51, 1417–1430, [https://doi.org/10.1175/1520-0469\(1994\)051<1417:HAVSOC>2.0.CO;2](https://doi.org/10.1175/1520-0469(1994)051<1417:HAVSOC>2.0.CO;2), 1994.
- Volk, C. M., Elkins, J. W., Fahey, D. W., Dutton, G. S., Gilligan, J. M., Loewenstein, M., Podolske, J. R., and Chan, K. R.: On the evaluation of source gas lifetimes from stratospheric observations, *J. Geophys. Res.*, 102, 25 543–25 564, 1997.
- Wang, K. Y. and Shallcross, D. E.: A modelling study of tropospheric distributions of the trace gases CFC13 and CH₃CCl₃ in the 1980s, *Annales Geophysicae*, 18, 972–986, <https://doi.org/10.1007/s00585-000-0972-3>, 2000.
- Waugh, D. W. and Hall, T. M.: Age of stratospheric air: Theory, observations, and models, *Rev. Geophys.*, 40, 1–27, 2002.
- Waugh, D. W. and Polvani, L. M.: Climatology of intrusions into the tropical upper troposphere, *Geophys. Res. Lett.*, 27, 3857–3860, 2000.
- Waugh, D. W., Crotwell, A. M., Dlugokencky, E. J., Dutton, G. S., Elkins, J. W., Hall, B. D., Hints, E. J., Hurst, D. F., Montzka, S. A., Mondeel, D. J., Moore, F. L., Nance, J. D., Ray, E. A., Steenrod, S. D., Strahan, S. E., and Sweeney, C.: Tropospheric SF₆: Age of air from the Northern Hemisphere midlatitude surface, *J. Geophys. Res.*, 118, 11 429–11 441, 2013.
- Webster, P. J. and Holton, J. R.: Cross-Equatorial Response to Middle-Latitude Forcing in a Zonally Varying Basic State, *Journal of the Atmospheric Sciences*, 39, 722–733, [https://doi.org/10.1175/1520-0469\(1982\)039<0722:CERTML>2.0.CO;2](https://doi.org/10.1175/1520-0469(1982)039<0722:CERTML>2.0.CO;2), 1982.
- WMO: Scientific assessment of ozone depletion: 2018, Global Ozone Research and Monitoring Project–Report No. 58, Geneva, Switzerland, 2018.



- Wu, X., Griessbach, S., and Hoffmann, L.: Equatorward dispersion of a high-latitude volcanic plume and its relation to the Asian summer monsoon: a case study of the Sarychev eruption in 2009, *Atmospheric Chemistry and Physics*, 17, 13 439–13 455, <https://doi.org/10.5194/acp-17-13439-2017>, 2017.
- 565 Wu, X., Yang, H., Waugh, D. W., Orbe, C., Tilmes, S., and Lamarque, J.-F.: Spatial and temporal variability of interhemispheric transport times, *Atmospheric Chemistry and Physics*, 18, 7439–7452, <https://doi.org/10.5194/acp-18-7439-2018>, 2018.
- Yan, X., Konopka, P., Ploeger, F., Podglajen, A., Wright, J. S., Müller, R., and Riese, M.: The efficiency of transport into the stratosphere via the Asian and North American summer monsoon circulations, *Atmospheric Chemistry and Physics*, 19, 15 629–15 649, <https://doi.org/10.5194/acp-19-15629-2019>, 2019.
- 570 Yang, H., Waugh, D. W., Orbe, C., Patra, P. K., Jöckel, P., Lamarque, J.-F., Tilmes, S., Kinnison, D., Elkins, J. W., and Dlugokencky, E. J.: Evaluating Simulations of Interhemispheric Transport: Interhemispheric Exchange Time Versus SF6 Age, *Geophysical Research Letters*, 46, 1113–1120, <https://doi.org/10.1029/2018GL080960>, 2019.